A Novel Simulation Model for Coded OFDM in Doppler Scenarios

Mario Poggioni, *Student Member, IEEE*, Luca Rugini, *Member, IEEE*, and Paolo Banelli, *Member, IEEE*

***Abstract*—This paper proposes a novel simulation model to characterize the bit-error rate (BER) performance of coded orthogonal frequency-division multiplexing (OFDM) systems that are affected by the Doppler spread. The proposed equivalent frequency-domain OFDM model (EFDOM) avoids the exact generation of the time-varying channel by introducing several parameters that summarize the statistical properties of the channel and of the intercarrier interference (ICI) that is generated by the time variation of the channel. Simulation results are used to prove that the proposed model can be used to accurately predict the BER of coded OFDM systems in Rayleigh and Rice doubly selective channels. An attractive feature of the proposed model is the significant reduction of the simulation time with respect to the exact model. We show by simulation that the simulation efficiency increases for channels with many multipath components, whereas it is independent of the size of the fast Fourier transform (FFT).**

***Index Terms*—Bit-error rate (BER) performance, coded orthogonal frequency-division multiplexing (OFDM), Doppler spread, intercarrier interference (ICI), simulation, time-varying fading channels.**

I. Introduction

ORTHOGONAL frequency-division multiplexing (OFDM) is a well-established technique for high-rate communications in frequency-selective fading channels due to its easy per-subcarrier equalization in the frequency domain [1]. Consequently, OFDM is widely used in many popular wireless standards, such as IEEE 802.16e, IEEE 802.11a, digital video broadcasting—terrestrial (DVB-T) and handheld (DVB-H), digital audio broadcasting (DAB), and terrestrial digital multimedia broadcasting (T-DMB) [2]–[5]. However, in high-mobility environments, the time variation (i.e., the Doppler spread) of mobile radio channels destroys the orthogonality of the OFDM subcarriers, leading to the so-called intercarrier interference (ICI) [6], [7]. If advanced time-varying equalization techniques are not used, the ICI can significantly degrade the performance of OFDM systems introducing bit-error rate (BER) floors that channel coding can only try to reduce [6]. Consequently, a statistical characterization of the ICI is necessary to analytically assess the BER performance.

Several previous works [6]–[8] have shown that, for *uncoded* OFDM systems, BER performance can be obtained by modeling the ICI as an additive white Gaussian noise (AWGN), whose average power can be derived in a closed form [6], [7], [9]. It was shown in [10] that the jointly Gaussian approximation of the ICI is good for phase-shift keying OFDM, whereas for nonconstant envelope constellations, such as quadrature amplitude modulation (QAM), the probability density function (pdf) of the ICI is a Gaussian mixture, i.e., a weighted sum of Gaussian functions. However, a more appropriate figure of merit of a communication system is the coded BER performance, and, consequently, we want to model the ICI in *coded* OFDM (COFDM) systems. We will show that a simple extension of the AWGN-like ICI model from which it is derived [8] is not adequate for assessing the BER performance of COFDM systems. Specifically, we will show that the channel power-delay profile, which does not affect the BER performance of uncoded systems [8], conversely, can greatly impact the coded BER performance.

The broader scope of this paper is to assess the BER of COFDM systems that use simple per-subcarrier equalization to combat the adverse effect of doubly selective channels. To this end, we introduce an equivalent frequency-domain OFDM model (EFDOM), which is capable of predicting with good accuracy the BER performance without replicating the entire OFDM transmitter–receiver chain. The main idea of the EFDOM is to replace the exact generation of the ICI by a computer-generated "BER-equivalent" ICI to speed up the simulation time while maintaining the same BER produced by the exact ICI realization. This equivalent ICI is obtained by a moment-matching technique that tries to keep only a few relevant moments of the true ICI, such as its power and its cross-correlation with the useful channel. A specific merit of our model is its capability to highly reduce the simulation time with respect to the simulation of the exact OFDM model. We will show that the saving in simulation time mainly depends on the number of channel paths and is almost independent of the size N of the fast Fourier transform (FFT). This new model could be used, for instance, to compare the BER of different OFDM-based standards, such as DVB-T/H, DAB, and T-DMB. However, the comparison among different standards, although important, would require a significant space, and it is partially addressed in [11].

The rest of this paper is organized as follows. Section II briefly describes the COFDM system model in time-varying multipath channels. We will refer to this model as the *exact model*. In Section III, we introduce our simplified model, i.e., the EFDOM, by explaining all the constraints that we impose in the ICI generation. The accuracy of the proposed model is validated in Section IV, which illustrates the BER comparison

Manuscript received October 27, 2006; revised September 10, 2007 and October 12, 2007. The review of this paper was coordinated by Prof. H.-C. Wu.

The authors are with the Department of Electronic and Information Engineering, University of Perugia, 06125 Perugia, Italy (e-mail: paolo.banelli@diei.unipg.it).

Color versions of one or more of the figures in this paper are available online at http://ieeexplore.ieee.org.

Digital Object Identifier 10.1109/TVT.2007.913178

between the exact and simplified models in many scenarios. Section V shows the simulation time saving due to the use of the EFDOM, and Section VI concludes this paper.

Notation: Bold uppercase (lowercase) letters denote matrices (column vectors); the superscripts *, ^{T}, and ^{H} denote the conjugation, the transpose, and the Hermitian transpose, respectively, whereas $\|\cdot\|^2$ and $\otimes$ denote the Frobenius norm and the Kronecker product, respectively. We use $[\mathbf{X}]_{i,j}$ to denote the (i,j)th entry of the matrix $\mathbf{X}$; $[\mathbf{X}]_i$ ($[\mathbf{x}]_i$) denotes the ith row (element) of the matrix $\mathbf{X}$ (vector $\mathbf{x}$); $\mathbf{I}_K$ and $\mathbf{1}_K$ denote the identity matrix and the all-ones column vector of size K, respectively, whereas $\mathbf{0}_{M\times N}$ is the $M \times N$ matrix with all the elements equal to zero. $\mathrm{Diag}(\mathbf{a})$ is a diagonal matrix with the entries of $\mathbf{a}$ on the diagonal, whereas $\mathrm{diag}(\mathbf{A})$ is the column vector containing the main diagonal of $\mathbf{A}$. $E[\cdot]$ is used to denote the statistical expectation, while $\mathbf{R_{xy}} = E[\mathbf{x}\mathbf{y}^H]$ represents the cross-correlation, and $\mathbf{C_{xy}} = \mathbf{R_{xy}} - E[\mathbf{x}]E[\mathbf{y}^H]$ the cross-covariance, between $\mathbf{x}$ and $\mathbf{y}$. Last, $\lceil\cdot\rceil$ indicates the integer ceiling function, whereas $a \bmod N$ stands for the remainder of the division of a by N.

II. Exact System Model

We describe in this section a well-established OFDM system characterization, in time-varying channels, which we refer to as the *exact* system model.

A. Channel Model

According to the COST 207 standard [12], the continuous channel $h_c(t,\tau)$ is modeled as a frequency-selective time-varying fading channel, which is assumed to be wide-sense stationary with uncorrelated scattering (WSSUS) [13]. The discrete-time complex-valued channel is obtained by sampling the continuous channel, as expressed by

$$h_l[k] = h_c(kT_S, lT_S), \quad l = 0, \ldots, L-1 \tag{1}$$

where $h_l[k]$ represents the time evolution of the lth tap, $L = \lceil \tau_{\mathrm{MAX}}/T_S \rceil + 1$ is the number of channel taps, T_S is the sampling period, τ_{MAX} is the maximum excess delay, and $\{P_l = E[|h_l[k]|^2] = \sigma_l^2 + |m_l|^2, l = 0, \ldots, L-1\}$ represents the power-delay profile of the WSSUS channel, where σ_l^2 is the variance, and m_l is the mean value of the lth tap. The COST 207 standard encompasses four multipath channels, i.e., the typical urban, the bad urban (BU), the hilly terrain, and the rural area (RA), where each path is modeled as a random process with Rayleigh statistics, except for the first path of the RA, which is characterized by a Rice envelope. The line-of-sight path in the RA has a deterministic value that is added to the first nonline-of-sight path of the channel. Each path is characterized by the autocorrelation $R((n-k)T_S) = E[h_c^*(kT_S)h_c(nT_S)] = |m_l|^2 + \sigma_l^2 J_0(2\pi f_D(n-k)T_S)$, where $J_0(\tau)$ is the zero-order Bessel function of the first kind, and f_D is the maximum Doppler frequency, which leads to the widely used Jakes' Doppler spectrum [14]. The taps are independent, and the time variation of the taps is obtained by the sum-of-sinusoids method described in [14]. We will focus on two scenarios—the BU for Rayleigh channels and the RA for Rice channels. It is worth noting that the former has a much longer power-delay profile (10 μs) than the latter (0.7 μs).

B. OFDM System Model

We consider the classical OFDM system with cyclic prefix (CP) and no interblock interference because we consider a CP length $L_{\mathrm{CP}} \geq L-1$ [15]. The received signal, after CP removal and FFT processing, can be written, with a notation that is similar to [15], as follows:

$$\mathbf{y}(n) = \mathbf{H}(n)\mathbf{x}(n) + \mathbf{w}(n). \tag{2}$$

In (2), $\mathbf{x}(n)$ is the frequency-domain transmitted vector, and $\mathbf{H}(n) = \mathbf{F}\tilde{\mathbf{H}}(n)\mathbf{F}^H$ is the frequency-domain channel matrix, where $\tilde{\mathbf{H}}(n)$ is the corresponding matrix in the time domain, whereas $\mathbf{F}$ is the unitary FFT matrix of size N. Thus, the noise $\mathbf{w}(n) = \mathbf{F}\tilde{\mathbf{w}}(n)$ in the frequency domain has the same statistics of the AWGN noise $\tilde{\mathbf{w}}(n)$ in the time domain.

In time-invariant channels, i.e., when $f_D = 0$, the matrix $\tilde{\mathbf{H}}(n) = \tilde{\mathbf{H}}$ is circulant, as expressed by $[\tilde{\mathbf{H}}]_{i,j} = h_{(i-j) \bmod N}[i + nN_T]$, where $N_T = N + L_{\mathrm{CP}}$. Thus, $\mathbf{H}(n) = \mathbf{H}$ is diagonal [15], [16] with entries corresponding to the channel frequency response $\mathbf{h} = \sqrt{N}\mathbf{F}[h_0, \ldots, h_{L-1}, \mathbf{0}_{1\times(N-L)}]^T$, which leads to the low-complexity per-subcarrier equalization that characterizes OFDM systems. However, if the channel is time varying, $\mathbf{H}(n)$ is no longer diagonal, and some ICI is introduced. To express the impact of ICI when simple time-invariant per-subcarrier (i.e., diagonal) equalizers are employed, it is helpful to express the time-variant channel matrices as follows:

$$\begin{aligned} \tilde{\mathbf{H}}(n) &= \tilde{\mathbf{H}}_U(n) + \tilde{\mathbf{H}}_I(n) \\ \mathbf{H}(n) &= \mathbf{H}_U(n) + \mathbf{H}_I(n) \end{aligned} \tag{3}$$

where the relations $\mathbf{H}_U(n) = \mathbf{F}\tilde{\mathbf{H}}_U(n)\mathbf{F}^H$ and $\mathbf{H}_i(n) = \mathbf{F}\tilde{\mathbf{H}}_i(n)\mathbf{F}^H$ link the frequency-domain with the time-domain channel matrices. In (3), $\tilde{\mathbf{H}}_U(n)$ represents the useful part of the time-domain channel matrix and is a circulant matrix whose elements are obtained by the time average of the channel in the nth OFDM block, which is expressed by $\overline{\mathbf{h}}_T(n) = N^{-1}\sum_{i=L_{\mathrm{CP}}+1}^{N_T} \mathbf{h}_T(i+nN_T)$, where $\mathbf{h}_T(i+nN_T) = [h_0(i+nN_T), \ldots, h_{L-1}(i+nN_T), 0, \ldots, 0]^T$. On the contrary, $\tilde{\mathbf{H}}_I(n) = \tilde{\mathbf{H}}(n) - \tilde{\mathbf{H}}_U(n)$ is the ICI generating matrix. By inserting (3) into (2), we obtain

$$\mathbf{y}(n) = \mathbf{H}_U(n)\mathbf{x}(n) + \mathbf{n}_{\mathrm{ICI}}(n) + \mathbf{w}(n) \tag{4}$$

where $\mathbf{y}_U(n) = \mathbf{H}_U(n)\mathbf{x}(n)$ represents the useful received signal, and

$$\mathbf{n}_{\mathrm{ICI}}(n) = \mathbf{H}_I(n)\mathbf{x}(n) \tag{5}$$

stands for the ICI that is introduced by the time-variant part $\mathbf{H}_I(n)$ of the channel matrix. By defining $\mathbf{h}_U(n) = \sqrt{N}\mathbf{F}\overline{\mathbf{h}}_T(n)$, it can be easily verified that

$$\mathbf{H}_U(n) = \mathrm{Diag}\left(\mathbf{h}_U(n)\right), \qquad \mathrm{diag}\left(\mathbf{H}_I(n)\right) = \mathbf{0}_{N\times 1}. \tag{6}$$

It is worth noting that $E[|[\mathbf{y}_U(n)]_i|^2] = 1 - E[|[\mathbf{n}_{\mathrm{ICI}}(n)]_i|^2] = 1 - P_{\mathrm{ICI}}\ \forall i$, where the ICI power P_{ICI} is expressed by [6]

$$P_{\mathrm{ICI}} = E\left[|[\mathbf{n}_{\mathrm{ICI}}(n)]_i|^2\right] = \frac{N-1}{N} - \frac{2}{N^2}\sum_{k=1}^{N-1} J_0\left(2\pi\frac{\overline{f}_D}{N}(N-k)\right) \quad (7)$$

where $\overline{f}_D$ is the normalized Doppler spread defined as $\overline{f}_D = f_D/\Delta f = f_c T_S N v/c$, Δf is the subcarrier separation, f_c is the carrier frequency, c is the speed of light and v is the vehicle speed. For simplicity, the reduction of the ICI power at the edge of the active bandwidth, due to switched-off subcarriers acting as guard bands [10], is not considered in (7). However, N here is quite large, and the expression in (7) is a very good approximation for nearly all the active subcarriers. Equation (7) is slightly pessimistic for just a few subcarriers at the edge of the spectrum. Thus, the use of (7) also for these subcarriers does not noticeably affect the average BER performance.

C. Channel Coding, Interleaving, and Equalization

We consider a rate-compatible punctured convolutional (RCPC) channel coding scheme with polynomial generator $G = [\,171 \quad 133\,]$ and 64 states [17]. For the decoding, we consider a soft Viterbi decoder with a four-bit quantization of the input signal. We assume that the bits at the output of the channel encoder are permuted by a bit interleaver and successively mapped to symbols that belong to an M-level constellation, such as quadrature phase shift keying (QPSK) and M-quadrature amplitude modulation (M-QAM). This stream of symbols is then permuted using a pseudorandom symbol interleaver with depth $D = N_S N_A$, where N_S is the number of OFDM blocks that correspond to the interleaver depth, and $N_A = N - N_G$ is the number of active subcarriers in a single OFDM block. We also assume that the RCPC codewords have a length that is equal to $n_b D$, with $n_b = \log_2 M$, i.e., equal to the depth of the symbol interleaver. This is motivated by the forced termination that is usually employed in the Viterbi decoding to attain manageable complexity [17]. In this paper, we will consider QPSK modulation, and hence, $n_b = 2$.

By denoting with $\underline{\mathbf{s}}$ the D-dimensional vector that represents the RCPC-coded symbol stream, we express the interleaved stream as $\underline{\mathbf{s}}_I = \underline{\mathbf{P}}\,\underline{\mathbf{s}}$, where $\underline{\mathbf{P}}$ is a square permutation matrix. The stream $\underline{\mathbf{s}}_I$ is then parsed in N_S blocks, each one of dimension N_A, which will be transmitted in different OFDM blocks. The nth block, which is denoted with $\mathbf{s}_I(n)$, can be expressed by $\mathbf{s}_I(n) = \mathbf{T}(n)\mathbf{s}_I$, where $\mathbf{T}(n) = [\mathbf{0}_{N_A\times(n-1)N_A}, \mathbf{I}_{N_A}, \mathbf{0}_{N_A\times(N_S-n)N_A}]$ for $n = 1, \ldots, N_S$. After the insertion of the frequency guard band by the matrix $\mathbf{G} = [\mathbf{0}_{N_A\times(N_G+1)/2}, \mathbf{I}_{N_A}, \mathbf{0}_{N_A\times(N_G-1)/2}]^T$, we can express the nth OFDM block that is transmitted in (2) as follows:

$$\mathbf{x}(n) = \mathbf{G}\mathbf{s}_I(n) = \mathbf{G}\mathbf{T}(n)\underline{\mathbf{P}}\,\underline{\mathbf{s}}. \quad (8)$$

By inserting (8) into (4), the received signal that is related to the nth OFDM block can be expressed by

$$\mathbf{y}(n) = \mathbf{H}_U(n)\mathbf{G}\mathbf{T}(n)\underline{\mathbf{P}}\,\underline{\mathbf{s}} + \mathbf{n}_{\mathrm{ICI}}(n) + \mathbf{w}(n). \quad (9)$$

We assume that the channel equalization is performed by using a diagonal time-invariant equalizer that compensates for the diagonal matrix $\mathbf{H}_U(n)$. Specifically, for the QPSK modulation considered in this paper, we compensate only for the estimated phase of the channel. This way, we can implicitly take into account the channel state information, thus allowing for better exploitation of soft convolutional decoding techniques, conceptually similar to [18].

D. Simulation of the Exact Model

To simulate the exact COFDM model, we should generate N_S OFDM blocks using (8) and successively transmit them through the time-variant channel using (2). Since the channel matrices $\{\mathbf{H}(n)\}_{n=1,\ldots,N_S}$ are correlated, the generation of the time-variant channel is generally very cumbersome, particularly when the number N of subcarriers is quite large or when the interleaver time span is very long (i.e., N_S is large). In addition, when the channel is time variant, each channel matrix $\tilde{\mathbf{H}}(n)$ is neither circulant nor Toeplitz. This means that the convolution between the transmitted signal and the channel, which is represented by the matrix multiplication in (2), cannot be performed using those FFT algorithms [19] that are usually adopted to speed up the simulation over time-invariant channels. As a result, the generation of the time-variant channel and its interaction with the data signal require the biggest part of the simulation time of the whole COFDM system.

III. EFDOM

To reduce the simulation time of COFDM systems, while maintaining the same BER performance, we develop a simple, accurate, and flexible simulation model that is based on a frequency-domain approximation of (4) rather than on the exact (2). Since we are interested in the coded BER performance, all the received vectors $\{\mathbf{y}(n)\}_{n=1,\ldots,N_S}$ that correspond to the same RCPC codeword $\underline{\mathbf{s}}_I$ should be considered together. Hence, let us group the received vectors $\{\mathbf{y}(n)\}_{n=1,\ldots,N_S}$ in a superblock $\mathbf{y} = [\mathbf{y}^T(1), \ldots, \mathbf{y}^T(N_S)]^T$ that considers all the N_S blocks that are related to the same time span of the symbol interleaver. This way, (9) becomes

$$\underline{\mathbf{y}} = \underline{\mathbf{H}}_U\underline{\mathbf{G}}\,\underline{\mathbf{P}}\,\underline{\mathbf{s}} + \underline{\mathbf{n}}_{\mathrm{ICI}} + \underline{\mathbf{w}} \quad (10)$$

where $\underline{\mathbf{H}}_U = \mathrm{Diag}(\underline{\mathbf{h}}_U)$, $\underline{\mathbf{h}}_U = [\mathbf{h}_U^T(1), \ldots, \mathbf{h}_U^T(N_S)]^T$, $\underline{\mathbf{G}} = \mathbf{I}_{N_S} \otimes \mathbf{G}$, $\underline{\mathbf{n}}_{\mathrm{ICI}} = [\mathbf{n}_{\mathrm{ICI}}^T(1), \ldots, \mathbf{n}_{\mathrm{ICI}}^T(N_S)]^T$, and $\underline{\mathbf{w}} = [\mathbf{w}^T(1), \ldots, \mathbf{w}^T(N_S)]^T$. From (10), it is clear that the useful part of the channel can be generated in a simple way because $\underline{\mathbf{H}}_U$ is diagonal. In other words, in the exact model, the time-consuming part is represented by the generation of $\underline{\mathbf{n}}_{\mathrm{ICI}}$ by means of (5). As a consequence, to reduce the computational complexity, (10) suggests to use a *statistically equivalent* vector $\underline{\mathbf{n}}_{\mathrm{ICI}}^{(E)}$ with a faster generation than the exact $\underline{\mathbf{n}}_{\mathrm{ICI}}$, preserving the average BER performance of the system. This is the main idea that will lead to our EFDOM.

We remark that a theoretical coded BER performance analysis would be a better alternative to the simulation model we

are going to introduce. Anyway, the analytical BER approach presents two obstacles. First, the BER analysis would require the knowledge of the joint pdf $f_{\underline{\mathbf{h}}_U,\underline{\mathbf{n}}_{\mathrm{ICI}}}(\underline{\mathbf{h}}_U,\underline{\mathbf{n}}_{\mathrm{ICI}})$, whose derivation is not easy to find. Second, the union bound technique, which is widely employed for the theoretical BER analysis of convolutionally coded systems, usually introduces too much approximation, particularly at a low SNR [20], [21].

To develop our model, we assume in our analysis that deinterleaving is performed before the equalization. Although, in a practical system, these two operations are reversed, our analysis is correct, because our time-invariant equalizer separately acts on each subcarrier by a diagonal matrix. Hence, the nonequalized received signal, after guard band removal and deinterleaving, can be written as follows:

$$\underline{\mathbf{z}} = \underline{\mathbf{P}}^T\underline{\mathbf{G}}^T\underline{\mathbf{y}} = \underline{\mathbf{A}}\,\underline{\mathbf{s}} + \underline{\mathbf{i}} + \underline{\mathbf{v}} \tag{11}$$

where $\underline{\mathbf{A}} = \underline{\mathbf{P}}^T\underline{\mathbf{G}}^T\underline{\mathbf{H}}_U\underline{\mathbf{G}}\,\underline{\mathbf{P}}$ is the diagonal matrix that represents the aggregate effect of the useful channel, guard bands, and interleaving, $\underline{\mathbf{i}} = \underline{\mathbf{P}}^T\underline{\mathbf{G}}^T\underline{\mathbf{n}}_{\mathrm{ICI}}$ is the ICI after the deinterleaver, and $\underline{\mathbf{v}} = \underline{\mathbf{P}}^T\underline{\mathbf{G}}^T\underline{\mathbf{w}}$ stands for the AWGN. Interestingly, the channel that directly impacts on the performance of the Viterbi decoder can be expressed by $\underline{\mathbf{a}} = \mathrm{diag}(\underline{\mathbf{A}}) = \underline{\mathbf{P}}^T\underline{\mathbf{G}}^T\underline{\mathbf{h}}_U$. Instead of the exact model of (11), the EFDOM generates *statistically equivalent* versions of the useful channel and of the ICI, as expressed by

$$\underline{\mathbf{z}}^{(E)} = \underline{\mathbf{A}}^{(E)}\underline{\mathbf{s}} + \underline{\mathbf{i}}^{(E)} + \underline{\mathbf{v}} \tag{12}$$

where $\underline{\mathbf{i}}^{(E)}$ is a suitable approximation of $\underline{\mathbf{i}}$, and the matrix $\underline{\mathbf{A}}^{(E)}$ is generated with the same statistics of the exact $\underline{\mathbf{A}}$. As we will detail, the generation of $\underline{\mathbf{a}}^{(E)} = \mathrm{diag}(\underline{\mathbf{A}}^{(E)})$ and of $\underline{\mathbf{i}}^{(E)}$ is quite fast. This way, the EFDOM avoids the time-consuming steps that appear during the simulation of the exact OFDM model. One is the generation of the exact time-varying channel over all the interleaver length D, which forces to generate (possibly) several channel taps for many time instants; the other is the time-variant convolution with the transmitted data signal.

In addition to the faster simulation, which will be justified later, a second merit of the EFDOM is the analytical insight on the effects of the ICI. Indeed, to maintain the model as simple as possible, the generation of $\underline{\mathbf{a}}^{(E)}$ and $\underline{\mathbf{i}}^{(E)}$ should be related to only a few parameters, such as the ICI power and cross-correlation, i.e., those statistical moments that mostly affect the coded BER performance. In some cases, the identification of these key parameters is based on theoretical considerations, whereas in other cases, it is based on intuitive arguments and validated by simulation of the exact model. In the following, we discuss each key parameter of the EFDOM.

A. Parameter 1: Useful Channel Vector

In Rayleigh and Rice scenarios, the useful channel vector $\underline{\mathbf{a}}$ is jointly Gaussian. Consequently, in the EFDOM, $\underline{\mathbf{a}}^{(E)}$ is generated as a complex jointly Gaussian random vector, with covariance matrix $\mathbf{C}_{\underline{\mathbf{aa}}} = \underline{\mathbf{P}}^T\underline{\mathbf{G}}^T\mathbf{C}_{\underline{\mathbf{h}}_U\underline{\mathbf{h}}_U}\underline{\mathbf{G}}\,\underline{\mathbf{P}}$, where $\mathbf{C}_{\underline{\mathbf{h}}_U\underline{\mathbf{h}}_U}$ is the covariance of the useful channel $\underline{\mathbf{h}}_U$. The size of the covariance matrix $\mathbf{C}_{\underline{\mathbf{aa}}}$ depends on the (finite) length of the interleaver, and it has a significant impact on the BER performance. Indeed, if the interleaver depth D is short, the covariance matrix $\mathbf{C}_{\underline{\mathbf{aa}}}$, due to the cross-correlation among consecutive elements of $\underline{\mathbf{a}}$, significantly departs from a diagonal structure and, consequently, reduces the correcting capabilities of the Viterbi decoder, as it happens in the exact model. On the contrary, for an infinite interleaving depth, $\mathbf{C}_{\underline{\mathbf{aa}}}$ approaches a scaled identity matrix because it contains a few diagonal elements that are different from zero, which are quite distant from one another. Exploiting the uncorrelated scattering assumption, and the same Doppler power spectrum density for all the channel taps, the covariance matrix $\mathbf{C}_{\underline{\mathbf{h}}_U\underline{\mathbf{h}}_U}$ can be expressed as follows (see Appendix A):

$$\mathbf{C}_{\underline{\mathbf{h}}_U\underline{\mathbf{h}}_U} = \overline{\mathbf{C}}_{\mathrm{norm}} \otimes \mathbf{C}_{\mathbf{h}_U(n)\mathbf{h}_U(n)} \tag{13}$$

where $\overline{\mathbf{C}}_{\mathrm{norm}}$ is the $N_S \times N_S$ covariance matrix of a power-normalized channel path, as expressed by

$$[\overline{\mathbf{C}}_{\mathrm{norm}}]_{n,k} = \frac{1}{N^2}\sum_{i=0}^{N-1}\sum_{j=0}^{N-1} J_0\left(\frac{2\pi\overline{f}_D}{N}\left((n-k)N+j-i\right)\right) \qquad n,k = 1,\ldots,N_S. \tag{14}$$

In (14), $\mathbf{C}_{\mathbf{h}_U(n)\mathbf{h}_U(n)} = N\mathbf{F}\mathbf{\Sigma}\mathbf{F}^H$, and $\mathbf{\Sigma}$ is a diagonal matrix, representing the power-delay profile, with nonzero entries only in its first L elements, as expressed by $[\mathbf{\Sigma}]_{l+1,l+1} = \sigma_l^2, 0 \le l \le L-1$. It is noteworthy that in (13), the effect of the Doppler spread, which is represented by $\overline{\mathbf{C}}_{\mathrm{norm}}$, is separated from the effect of the power-delay profile contained in $\mathbf{C}_{\mathbf{h}_U(n)\mathbf{h}_U(n)}$.

From a practical point of view, $\underline{\mathbf{a}}^{(E)}$ can be generated as a linear transformation of a computer-generated white Gaussian random vector $\underline{\mathbf{g}}_1$, with zero mean and covariance $\mathbf{C}_{\underline{\mathbf{gg}}} = \mathbf{I}_{N_SN}$, by exploiting the knowledge of $\mathbf{C}_{\underline{\mathbf{aa}}}$, the eigenvalue decomposition (EVD) technique [16], and the Kronecker product property $\mathbf{AC}\otimes\mathbf{BD} = (\mathbf{A}\otimes\mathbf{B})(\mathbf{C}\otimes\mathbf{D})$. Specifically, by the EVD $\overline{\mathbf{C}}_{\mathrm{norm}} = \mathbf{U}_{\mathrm{norm}}\mathbf{\Lambda}_{\mathrm{norm}}\mathbf{U}_{\mathrm{norm}}^H$, the EFDOM generates

$$\underline{\mathbf{h}}_U^{(E)} = \left(\mathbf{U}_{\mathrm{norm}}\mathbf{\Lambda}_{\mathrm{norm}}^{1/2}\otimes\mathbf{F}\mathbf{\Sigma}^{1/2}\right)\underline{\mathbf{g}}_1 + E[\underline{\mathbf{h}}_U] \tag{15}$$

$$\underline{\mathbf{A}}^{(E)} = \mathrm{Diag}\left(\underline{\mathbf{a}}^{(E)}\right) = \mathrm{Diag}\left(\underline{\mathbf{P}}^T\underline{\mathbf{G}}^T\underline{\mathbf{h}}_U^{(E)}\right). \tag{16}$$

B. Parameter 2: ICI Vector

Within the interleaver depth, the ICI vector $\underline{\mathbf{i}}$ is very close to a complex jointly Gaussian random vector, as confirmed by the theoretical models that are used to analytically derive the uncoded BER [8]. This is true particularly for QPSK [10] or when the FFT size N is large enough to invoke the central limit theorem (e.g., $N \ge 64$). In addition, $\underline{\mathbf{i}}$ is not white. Its covariance $\mathbf{C}_{\underline{\mathbf{ii}}}$, which is derived in Appendix B, depends on the channel only through the Doppler spread and does not depend on the power-delay profile.

In principle, we could generate a jointly Gaussian random vector, with covariance $\mathbf{C}_{\underline{\mathbf{ii}}}$ and independent from $\underline{\mathbf{a}}^{(E)}$, similarly to the generation of the useful channel. Indeed, as shown in [10], this approach is accurate enough to model the uncoded BER performance, whose dependence on the power-delay profile is almost absent. Moreover, this approach

would be highly accurate also for the coded BER performance when the interleaver length tends to infinity. However, in practical cases, where the interleaver time-span D is finite, the superblock ICI power $\overline{P}_{\rm ICI}$, which is defined as $\overline{P}_{\rm ICI} = \|\underline{\mathbf{i}}\|^2/(N_S N_A)$, does not coincide with the statistical power $P_{\rm ICI}$ in (7). By observing the extensive simulation results that are obtained with the exact model, we found out that the variability of $\overline{P}_{\rm ICI}$ from superblock to superblock plays an important role and cannot be neglected. As a consequence, our EFDOM has to include in its model also the variability of the superblock ICI power.

Intuitively, the variability of $\overline{P}_{\rm ICI}$ depends on the correlation of the channel realizations during the interleaver time span. Thus, different channel realizations produce different values of $\overline{P}_{\rm ICI}$ and, therefore, different BER performances. A possible way to include this dependence could be by linking the covariance $\mathbf{C}_{\underline{\mathbf{i}}^{(E)}\underline{\mathbf{i}}^{(E)}}$ of the modeled ICI $\underline{\mathbf{i}}^{(E)}$ to the actual channel realization. However, this method would require the generation of the time-varying channel realization over all the interleaver time span, which we want to avoid. Therefore, in the EFDOM, we choose an alternative way, and we model the effect of the superblock ICI power $\overline{P}_{\rm ICI}$ by a random variable. Specifically, we define

$$\varphi = \frac{\overline{P}_{\rm ICI}}{P_{\rm ICI}} = \frac{\|\underline{\mathbf{i}}\|^2}{N_A N_S P_{\rm ICI}} \tag{17}$$

as the ratio between the superblock ICI power $\overline{P}_{\rm ICI}$ and the statistical ICI power $P_{\rm ICI}$ expressed by (7). This ratio should be used as a multiplicative correction factor on the ICI power. Consequently, we split the ICI vector as follows:

$$\underline{\mathbf{i}}^{(E)} = \sqrt{\varphi^{(E)}}\,\hat{\underline{\mathbf{i}}}^{(E)} \tag{18}$$

where the two independent parameters $\varphi^{(E)}$ and $\hat{\underline{\mathbf{i}}}^{(E)}$ model the superblock ICI power ratio and the statistical properties of the ICI, respectively. In the EFDOM, we impose that the random variable $\varphi^{(E)}$ has approximately the same pdf of φ in (17), as will be discussed later on. This way, $E[\varphi^{(E)}] = E[\varphi] = 1$, and, therefore, $\underline{\mathbf{i}}^{(E)}$ and $\hat{\underline{\mathbf{i}}}^{(E)}$ will have the same covariance, as expressed by $\mathbf{C}_{\underline{\mathbf{i}}^{(E)}\underline{\mathbf{i}}^{(E)}} = E[\varphi^{(E)}]\mathbf{C}_{\hat{\underline{\mathbf{i}}}^{(E)}\hat{\underline{\mathbf{i}}}^{(E)}}$. As a result, the EFDOM generates a vector $\hat{\underline{\mathbf{i}}}^{(E)}$ such that its covariance $\mathbf{C}_{\hat{\underline{\mathbf{i}}}^{(E)}\hat{\underline{\mathbf{i}}}^{(E)}}$ is equal to the covariance $\mathbf{C}_{\underline{\mathbf{i}}\underline{\mathbf{i}}}$ of the exact ICI, which is derived in Appendix B. As already explained for the generation of $\underline{\mathbf{a}}^{(E)}$, we start from the generation of a jointly Gaussian random vector $\underline{\mathbf{g}}_2$, and exploiting the EVD $\mathbf{C}_{\underline{\mathbf{i}}\underline{\mathbf{i}}} = \mathbf{U}_{\underline{\mathbf{i}}}\mathbf{\Lambda}_{\underline{\mathbf{i}}}\mathbf{U}_{\underline{\mathbf{i}}}^H$, we generate $\hat{\underline{\mathbf{i}}}^{(E)}$ as expressed by

$$\hat{\underline{\mathbf{i}}}^{(E)} = \mathbf{U}_{\underline{\mathbf{i}}}\mathbf{\Lambda}_{\underline{\mathbf{i}}}^{1/2}\underline{\mathbf{g}}_2. \tag{19}$$

As far as φ in (17) is concerned, the exact derivation of its pdf $f_\varphi(\varphi)$ is very difficult. Anyway, $f_\varphi(\varphi)$ can be accurately approximated resorting to some intuitive considerations. We already know that the superblock ICI power $\overline{P}_{\rm ICI}$ depends on the time-variant part of the channel taps $\{|h_l[k] - m_l|^2\}$, where the channel elements $\{h_l[k]\}$ are complex Gaussian random variables, and the mean tap values $\{m_l\}$ are all zero for Rayleigh channels but not for Rice channels. Therefore, looking at (17), we expect the pdf $f_\varphi(\varphi)$ to be close to the pdf of the sum of (possibly correlated) exponential random variables. By exploiting the simulation results of the exact model, we found a close match between the histograms that approximate $f_\varphi(\varphi)$ and the pdf of the useful channel power in the superblock. As a consequence, the EFDOM selects

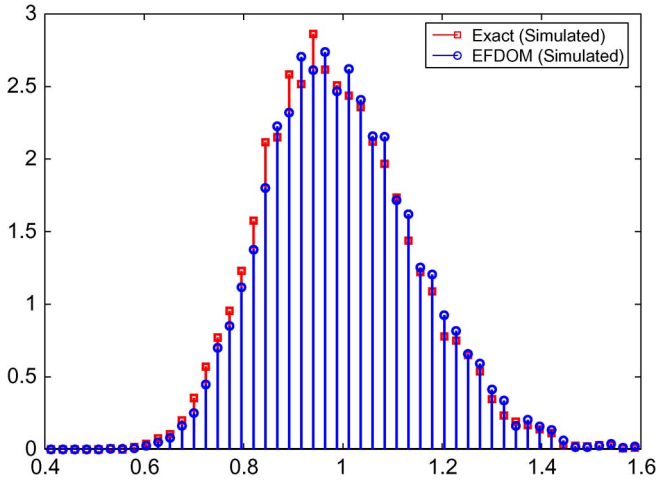

Fig. 1. Comparison between the simulated pdf of φ and of $\varphi^{(E)}$ (BU, $\overline{f}_D = 0.14$, and $N_S = 4$).

$$\varphi^{(E)} = \frac{1}{N_S}\sum_{n=1}^{N_S}\sum_{l=0}^{L-1}\left|h_l^{(E)}[n] - m_l\right|^2 \tag{20}$$

where $h_l^{(E)}[n]$ represents the lth tap of an equivalent channel that has the same power-delay profile and the same Doppler spread of the true channel. Since the time-variation index n of $h_l^{(E)}[n]$ changes on an OFDM-block basis, the equivalent channel is undersampled by a factor $N_T = N + L_{\rm CP}$ with respect to the true channel. As a consequence, the generation of the equivalent channel in the EFDOM is, by far, faster than that of the true channel in the exact model.

Figs. 1 and 2 show the close match between the histograms that estimate $f_\varphi(\varphi)$ and $f_{\varphi^{(E)}}(\varphi^{(E)})$. Interestingly, when $N_S = 1$, the pdf $f_{\varphi^{(E)}}(\varphi^{(E)})$ can be calculated in closed form, as detailed in Appendix C.

C. Parameter 3: Cross-Correlation Between the Useful Channel and the ICI

Thus far, we have separately considered the main statistical moments of $\underline{\mathbf{a}}^{(E)}$ and $\underline{\mathbf{i}}^{(E)}$. However, the ICI $\underline{\mathbf{i}}$ is generated by the channel and, therefore, could be correlated with the useful channel $\underline{\mathbf{h}}_U$. Since this correlation can have a nonnegligible impact on the BER performance, we will accordingly modify the EFDOM. To be precise, the EFDOM should impose the cross covariance $\mathbf{C}_{\underline{\mathbf{a}}^{(E)}\underline{\mathbf{i}}^{(E)}} = \mathbf{C}_{\underline{\mathbf{a}}\underline{\mathbf{i}}}$, which is an $N_S N_A \times N_S N_A$ matrix. However, this multidimensional constraint would highly complicate the simulation model. Therefore, to keep the model simple, we want to impose a single parameter.

Clearly, the coded BER performance on a superblock will depend on the total power of the useful signal, of the ICI, and

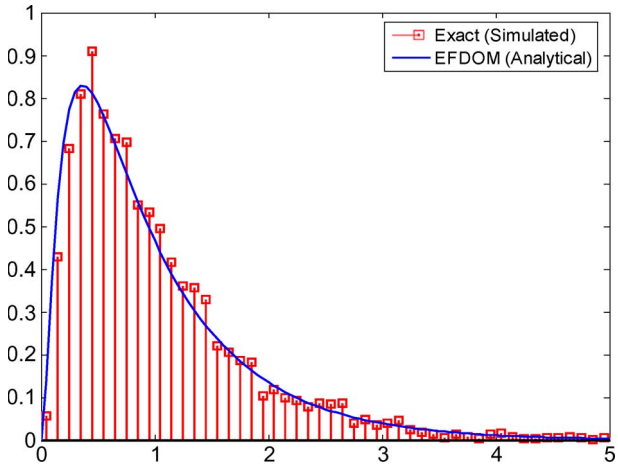

Fig. 2. Comparison between the pdf of φ (simulated) and $\varphi^{(E)}$ (analytical) (RA, $\overline{f}_D = 0.14$, and $N_S = 1$).

of the noise in that superblock. A meaningful parameter that captures the role played by all these quantities is the superblock signal-to-interference-plus-noise ratio (SINR), as expressed by

$$\overline{\text{SINR}} = \frac{\|\underline{\mathbf{A}}\,\underline{\mathbf{s}}\|^2}{\|\underline{\mathbf{i}}\|^2 + \|\underline{\mathbf{v}}\|^2}. \tag{21}$$

For a given statistical SNR, due to the high number N of subcarriers, the superblock noise power term $\|\underline{\mathbf{v}}\|^2$ can be considered as constant for every superblock with high accuracy. Therefore, the most important joint statistical moment that is related to the superblock SINR should be the correlation between the superblock energies $\|\underline{\mathbf{a}}\|^2$ and $\|\underline{\mathbf{i}}\|^2$. Consequently, let us consider $\overline{\text{SINR}}$ in (21) as a random variable that assumes different values for different superblocks, and let us define the superblock correlation coefficient as follows:[1]

$$\rho_P = \frac{E\left[\|\underline{\mathbf{A}}\,\underline{\mathbf{s}}\|^2\|\underline{\mathbf{i}}\|^2\right] - E\left[\|\underline{\mathbf{A}}\,\underline{\mathbf{s}}\|^2\right]E\left[\|\underline{\mathbf{i}}\|^2\right]}{\sqrt{E\left[\left(\|\underline{\mathbf{A}}\,\underline{\mathbf{s}}\|^2 - E\left[\|\underline{\mathbf{A}}\,\underline{\mathbf{s}}\|^2\right]\right)^2\right]E\left[\left(\|\underline{\mathbf{i}}\|^2 - E\left[\|\underline{\mathbf{i}}\|^2\right]\right)^2\right]}}. \tag{22}$$

To understand the impact of the correlation coefficient ρ_P on the BER performance, let us assume a sufficiently high statistical SNR, so that $\|\underline{\mathbf{v}}\|^2$ is small compared to $\|\underline{\mathbf{A}}\,\underline{\mathbf{s}}\|^2$. When ρ_P is low, the random variable $\overline{\text{SINR}}$ in (21) will have a high variance from a superblock to another, whereas for $\rho_P \to 1$, $\overline{\text{SINR}}$ will have a lower variance. Clearly, the BER performance in the former case is worse than in the latter case. Indeed, when the mean SINR $E[\overline{\text{SINR}}]$ is fixed, a high variance of $\overline{\text{SINR}}$ implies that there are many OFDM signal realizations with low values of $\overline{\text{SINR}}$ and many others with high values of $\overline{\text{SINR}}$. On the contrary, a low variance of $\overline{\text{SINR}}$ implies that all the realizations have an $\overline{\text{SINR}}$ that is close to the mean SINR $E[\overline{\text{SINR}}]$. Since the BER increase due to low SINR values is superior to the BER reduction that is guaranteed by high SINR values, the net effect is a worse BER with respect to the situation when the SINR is characterized by a low variance [22].

The correlation coefficient ρ_P is analytically calculated in Appendix D. To impose this correlation coefficient, the EFDOM first generates two independent jointly Gaussian vectors $\underline{\mathbf{g}}_a$ and $\underline{\mathbf{g}}_i$ and then exploits the EVD of

$$\mathbf{C}_{\rho_P} = \begin{bmatrix} \mathbf{I}_{N_S N_A} & \sqrt{\rho_P}\,\mathbf{I}_{N_S N_A} \\ \sqrt{\rho_P}\,\mathbf{I}_{N_S N_A} & \mathbf{I}_{N_S N_A} \end{bmatrix} = \begin{bmatrix} 1 & \sqrt{\rho_P} \\ \sqrt{\rho_P} & 1 \end{bmatrix} \otimes \mathbf{I}_{N_S N_A}. \tag{23}$$

The EVD $\mathbf{C}_{\rho_P} = \mathbf{U}_{\rho_P}\mathbf{\Lambda}_{\rho_P}\mathbf{U}_{\rho_P}^H$ can be easily derived as follows:

$$\mathbf{U}_{\rho_P} = \frac{1}{\sqrt{2}}\begin{bmatrix} \mathbf{I}_{N_S N_A} & -\mathbf{I}_{N_S N_A} \\ \mathbf{I}_{N_S N_A} & \mathbf{I}_{N_S N_A} \end{bmatrix}$$
$$\mathbf{\Lambda}_{\rho_P} = \begin{bmatrix} (1+\sqrt{\rho_P})\mathbf{I}_{N_S N_A} & \mathbf{0}_{N_S N_A \times N_S N_A} \\ \mathbf{0}_{N_S N_A \times N_S N_A} & (1-\sqrt{\rho_P})\mathbf{I}_{N_S N_A} \end{bmatrix} \tag{24}$$

where we exploited the following EVD:

$$\begin{bmatrix} 1 & \sqrt{\rho_P} \\ \sqrt{\rho_P} & 1 \end{bmatrix} = \frac{1}{2}\begin{bmatrix} 1 & -1 \\ 1 & 1 \end{bmatrix}\begin{bmatrix} 1+\sqrt{\rho_P} & 0 \\ 0 & 1-\sqrt{\rho_P} \end{bmatrix}\begin{bmatrix} 1 & -1 \\ 1 & 1 \end{bmatrix}^T. \tag{25}$$

From (23), it is clear that the correlation coefficient ρ_P is imposed subcarrier by subcarrier. Although this approach reduces the simulation complexity, in practice, the correlation holds true only on the average. In other words, we wanted to impose ρ_P as the correlation coefficient between the average power, which does not necessarily require an analogous correlation on each subcarrier. As a consequence, after imposing (23), the EFDOM employs a pseudorandom $N_S N_A \times N_S N_A$ permutation matrix $\tilde{\underline{\mathbf{P}}}$ to scramble the ICI samples among different subcarriers. This procedure is expressed by

$$\begin{bmatrix} \underline{\mathbf{g}}_1 \\ \underline{\mathbf{g}}_2 \end{bmatrix} = \begin{bmatrix} \mathbf{I}_{N_S N_A} & \mathbf{0}_{N_S N_A \times N_S N_A} \\ \mathbf{0}_{N_S N_A \times N_S N_A} & \tilde{\underline{\mathbf{P}}} \end{bmatrix}(\mathbf{M} \otimes \mathbf{I}_{N_S N_A})\begin{bmatrix} \underline{\mathbf{g}}_a \\ \underline{\mathbf{g}}_i \end{bmatrix}$$
$$\mathbf{M} = \frac{\sqrt{2}}{2}\begin{bmatrix} \sqrt{1+\sqrt{\rho_P}} & -\sqrt{1-\sqrt{\rho_P}} \\ \sqrt{1+\sqrt{\rho_P}} & \sqrt{1-\sqrt{\rho_P}} \end{bmatrix} \tag{26}$$

where the output vectors $\underline{\mathbf{g}}_1$ and $\underline{\mathbf{g}}_2$ are those used as input vectors for the generation of $\underline{\mathbf{a}}^{(E)}$ and $\underline{\mathbf{i}}^{(E)}$ in (16) and (18), respectively. Interestingly, when $\rho_P \to 0$, as expressed by

$$E\left[\|\underline{\mathbf{A}}\,\underline{\mathbf{s}}\|^2\|\underline{\mathbf{i}}\|^2\right] \approx E\left[\|\underline{\mathbf{A}}\,\underline{\mathbf{s}}\|^2\right]E\left[\|\underline{\mathbf{i}}\|^2\right] \tag{27}$$

the coefficient ρ_P can be neglected, and $\mathbf{C}_{\rho_P}$ can be approximated by an identity matrix. In this case, the two vectors $\underline{\mathbf{g}}_1$ and $\underline{\mathbf{g}}_2$ in (26) can be directly replaced by the two independent jointly Gaussian vectors $\underline{\mathbf{g}}_a$ and $\underline{\mathbf{g}}_i$, respectively. This situation occurs when the interleaver spans a single OFDM block, i.e., when $N_S = 1$, as we analytically derived in Appendix D and verified by simulations. Anyway, ρ_P can be neglected also when the interleaver depth is very long, or the Doppler spread is very high, such that each channel realization can be considered as ergodic over the interleaver time-span D.

Summarizing, we have identified a few parameters that affect the BER performance. These parameters are the autocovariance

[1]We consider the superblock received signal energy $\|\underline{\mathbf{A}}\,\underline{\mathbf{s}}\|^2$ instead of the superblock useful channel energy $\|\underline{\mathbf{a}}\|^2$; however, these values are very close to each other. Moreover, for QPSK data, $\|\underline{\mathbf{A}}\,\underline{\mathbf{s}}\|^2 = \|\underline{\mathbf{a}}\|^2$.

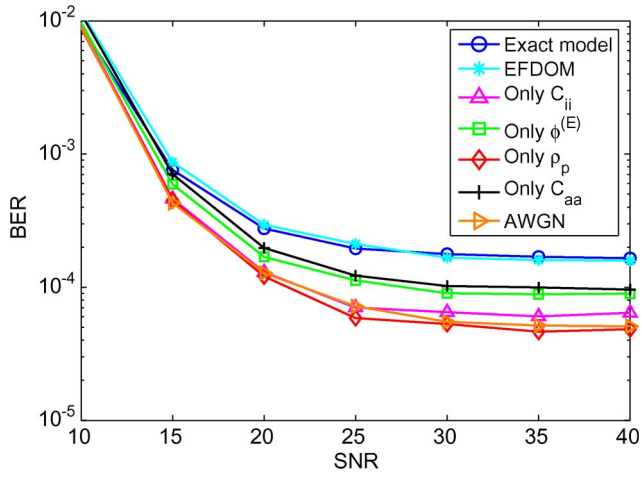

Fig. 3. Effect of the EFDOM parameters on the coded BER (BU, $\overline{f}_D = 0.28$, $N = 2048$, and CR 1/2).

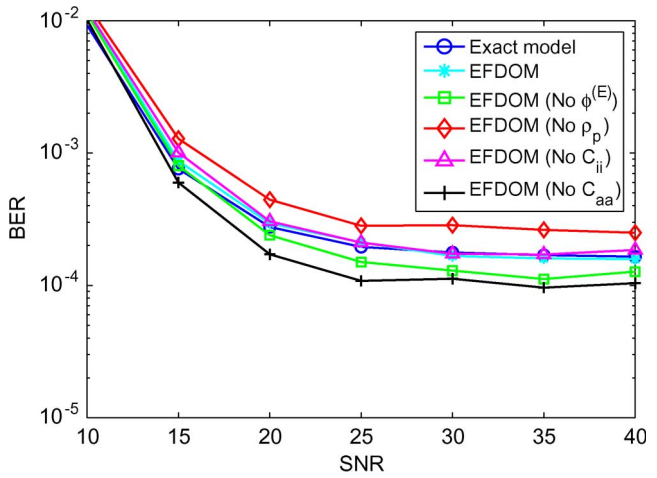

Fig. 4. Effect of the removal of a single EFDOM parameter (BU, $\overline{f}_D = 0.28$, $N = 2048$, and CR 1/2).

$\mathbf{C}_{\underline{\mathbf{h}}_U \underline{\mathbf{h}}_U}$ of the useful channel, the autocovariance $\mathbf{C}_{\underline{\mathbf{ii}}}$ of the ICI, the ratio φ between the superblock ICI power and the statistical ICI power, and the correlation coefficient ρ_P between the superblock useful signal power and the superblock ICI power. By (12), the EFDOM generates the nonequalized received signal (including symbol deinterleaving), where the quantities in (12) are obtained using (15), (16), (18)–(20), and (26).

We remark that the EFDOM is an inner step. Hence, to simulate the whole COFDM system, the other operations should be simulated as in the exact model. Specifically, before using the EFDOM, we should simulate channel coding, bit interleaving, and mapping, whereas after the EFDOM, we should perform equalization, demapping, bit deinterleaving, and channel decoding.

IV. EFDOM versus Exact Model: BER Performance

In this section, we validate the proposed EFDOM by comparing its BER with that one obtained using the exact model for different FFT sizes N. We assume that the frequency guard subcarriers are $N_G = 3N/16$. We also fix the product $NN_S = 8192$, which means that the interleaver length has been fixed to $D = N_A N_S = 13NN_S/16 = 6656$ complex symbols.

Fig. 3 plots the BER of a COFDM system for $N = 2048$ ($N_S = 4$) assuming a BU channel [12] with a normalized Doppler spread of $\overline{f}_D = 0.28$. For a DVB-H scenario, where the sampling time is $T_S = 0.125$ μs, and the carrier frequency is $f_c = 1.4$ GHz, this Doppler spread corresponds to $v = 840$ km/h. This unrealistic value for a DVB-H system has been chosen to obtain a high Doppler spread and, consequently, high BER floors, which better highlight the role played by the ICI and its accurate modeling by the EFDOM. Fig. 3 displays the BER estimates that are obtained with the exact model (circles), the EFDOM (stars), a model without any parameter of the EFDOM (right triangles), which can be used to derive uncoded BER performance [8], and four partial EFDOMs, each one obtained considering just one of the four parameters that characterize the EFDOM—$\varphi^{(E)}$ (squares), ρ_P (diamonds), $\mathbf{C}_{\underline{\mathbf{ii}}}$ (triangles), and $\mathbf{C}_{\underline{\mathbf{aa}}}$ (crosses). With this representation, it is possible to separately appreciate the importance of each parameter for the accuracy of the EFDOM. First, it is worth noting the excellent match between the BER performance that is obtained with the exact model and with the EFDOM, particularly between the BER floors. The importance of the parameters $\mathbf{C}_{\underline{\mathbf{aa}}}$ and $\varphi^{(E)}$ is clearly evident in Fig. 3. Specifically, the parameter $\mathbf{C}_{\underline{\mathbf{aa}}}$ imposes the autocovariance of the useful channel, which affects the effectiveness of the convolutional code, by possibly enhancing the probability to have error bursts at the input of the soft Viterbi decoder.

Fig. 3 shows that none of the four parameters alone is able to accurately model BER performance. It is difficult, however, to predict the separate effect on the BER floors of each single parameter, which can change with the simulation scenario, e.g., with the delay spread (RA or BU), the Doppler spread, and so forth. This fact is better clarified by the curve in Fig. 3, which is obtained with the partial EFDOM that considers only the parameter ρ_P (diamonds). Indeed, the parameter ρ_P alone leads to an underestimation of the BER floor because it reduces the variance of the average SINR on a superblock, as explained in Section III. This means that if we consider, for instance, the partial EFDOM with $\mathbf{C}_{\underline{\mathbf{aa}}}$, and we add the other two parameters $\mathbf{C}_{\underline{\mathbf{ii}}}$ and $\varphi^{(E)}$, we end up with a new partial EFDOM that conversely *overestimates* the BER floor, as shown in Fig. 4. The introduction of the fourth parameter ρ_P pushes back the BER floor to the exact one.

Fig. 5 plots the BER performance of a COFDM system with $N = 256$ and $N_S = 32$ in an RA channel. The normalized Doppler spreads are $\overline{f}_D = 0.009$ and $\overline{f}_D = 0.017$. Also, in this case, we can observe a very good match between the performance of the EFDOM and of the exact model. Specifically, the BER performance that is obtained with the EFDOM is very close to that obtained with the exact model for all the code rates and the Doppler spreads we considered. These curves are very interesting because they show an opposite behavior with respect to the uncoded BER performance [8], that is, a lower BER for *higher* Doppler spreads. This is due to the fact that, in this scenario, with $N = 256$ and $N_S = 32$, the OFDM

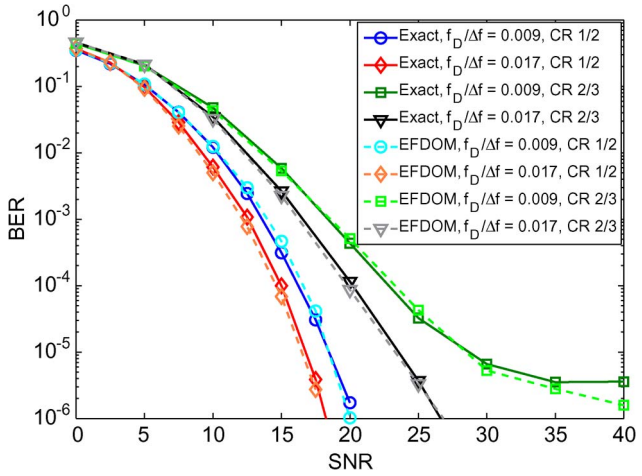

Fig. 5. Coded BER comparison between the EFDOM and the exact model (RA, $N = 256$).

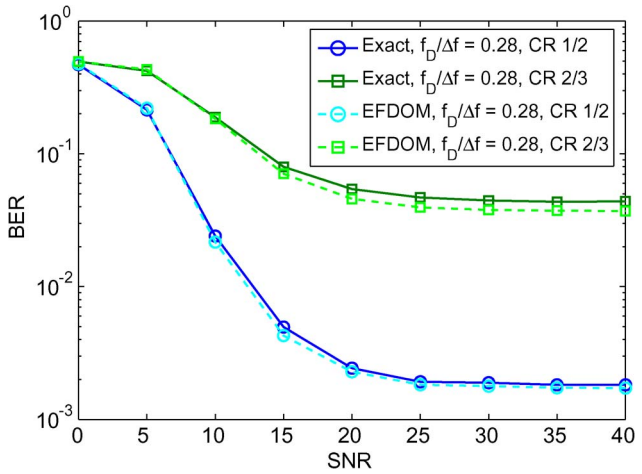

Fig. 6. Coded BER comparison between the EFDOM and the exact model (BU, $N = 8192$).

system is more capable of exploiting the time diversity that is offered by the time-variant channel with respect to $N = 8192$ and $N_S = 1$. Indeed, when $N = 8192$ and $N_S = 1$, there is only a set of 8192 useful frequency channel values with a frequency correlation that is imposed by the channel power-delay profile. Using $N_S > 1$ lets the system to have N useful frequency channels every OFDM symbol that are N_S times less correlated with one another. Moreover, the interleaver works on different useful frequency channel vectors, where each one is obtained from a different OFDM block. Because of the channel time variation, these channel vectors have a time correlation that decreases for higher Doppler spreads. This way, the system with $N_S > 1$ is capable to significantly reduce the BER floors by coding, which can benefit from the increased time diversity. All these observations are captured by the EFDOM by imposing the covariance matrix $\mathbf{C}_{\underline{\mathbf{aa}}}$, which we derive in Appendix A, showing its separate dependence on the power-delay profile and on the Doppler spread.

Figs. 6 and 7 plot the BER of a COFDM system with $N = 8192$ and $N_S = 1$ in a BU and in an RA channel (with Rice factor $K = 0$ dB, as defined in [12]), respectively. In this

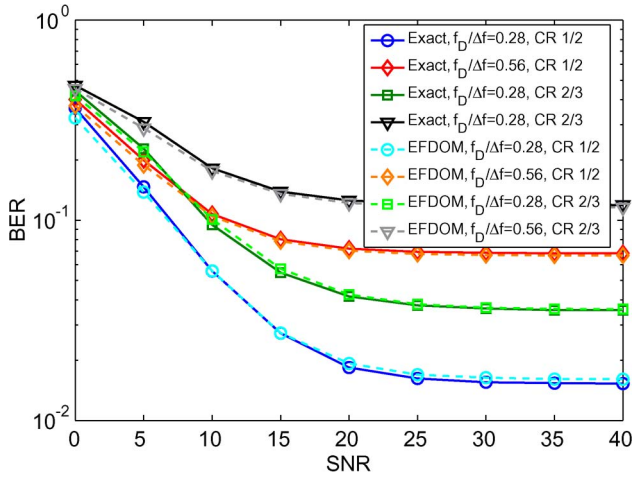

Fig. 7. Coded BER comparison between the EFDOM and the exact model (RA, $N = 8192$).

case, the interleaver works on a single OFDM block, i.e., only in the frequency domain, and the normalized Doppler spreads are $\overline{f}_D = 0.56$ and $\overline{f}_D = 0.28$. These values would correspond to an 8K DVB-T/H system that, for a 7-MHz bandwidth and a carrier frequency $f_c = 1.4$ GHz, is moving at speeds equal to $v = 210$ km/h and $v = 420$ km/h. Clearly, with this high Doppler spread, the ICI has a very high power (specifically, for a Rayleigh channel, $P_{\mathrm{ICI}} \cong 0.38$ for $\overline{f}_D = 0.56$), which makes it almost impossible for a per-subcarrier channel equalizer to get rid of the ICI, which produces a high BER at the Viterbi decoder output. However, we observe that for a Rice channel with $K = 0$ dB, the ICI power is reduced by 3 dB (because it depends only on the scattered part of the channel), and the Viterbi decoder is able to reduce the BER despite the high Doppler spread. This is why, in Fig. 6, we show the BER performance in the BU channel only for $\overline{f}_D = 0.28$, whereas Fig. 7 includes also $\overline{f}_D = 0.56$ for the RA channel. From Fig. 6, we can also notice very good accuracy of the EFDOM BER estimates in this scenario. Similar considerations hold true for Fig. 7, which illustrates the BER performance in the RA channel. Although, for $\overline{f}_D = 0.56$, the BER performance in a Rice channel is much better than in a Rayleigh one, as expected by the previous considerations, we observe a completely different behavior for $\overline{f}_D = 0.28$, which still permits correct performance of the convolutional decoder, also with per-subcarrier equalization. In this case, the *coded* BER performance in a Rayleigh channel, such as the BU, can significantly outperform the coded BER in a Rice channel such as the RA, despite the higher ICI power, due to the different power-delay profile characteristics of the two channels. This confirms the importance of the power-delay profile for the coded BER performance, whereas it is irrelevant for the uncoded BER [8].

V. EFDOM versus Exact Model: Simulation Time

The EFDOM greatly enhances the efficiency of the simulation of a COFDM model because the generation of $\underline{\mathbf{a}}^{(E)}$ for the useful channel and $\underline{\mathbf{i}}^{(E)}$ for the ICI is much faster than the generation of the true vectors $\underline{\mathbf{a}}$ and $\underline{\mathbf{i}}$. Indeed, the generation of the true vectors requires the generation of the

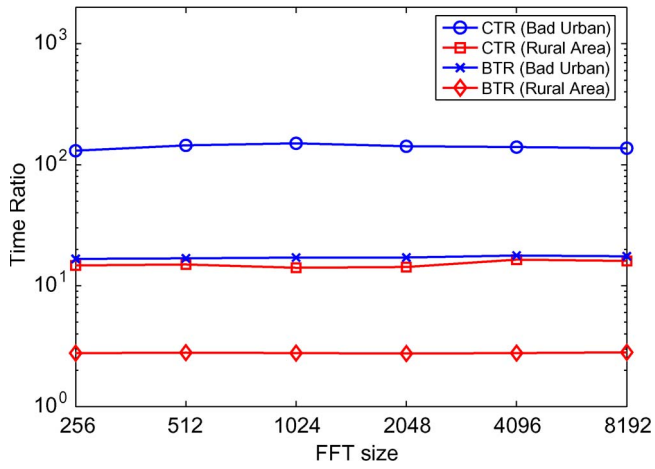

Fig. 8. CTR and BTR for different FFT sizes.

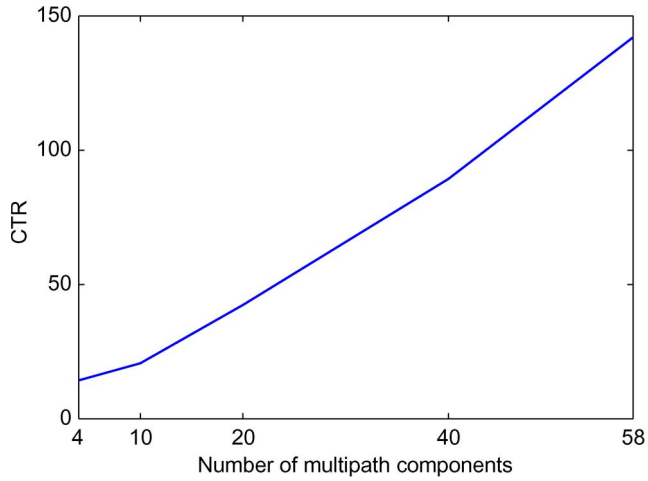

Fig. 9. CTR for different numbers of multipath components.

exact time variability of the channel taps in the time domain. This corresponds to the generation of $L(N + L_{\mathrm{CP}})N_S$ samples per simulation iteration, whereas the EFDOM generates only $(2N + L)N_S$ samples per iteration. Clearly, the efficiency of the EFDOM increases with the number L of channel taps. It is worth noting that the generation of the useful channel and of the ICI directly in the frequency domain also avoids the *time-varying convolution* of the channel with the data, which, in the simulation of the exact model, is the most time-consuming operation, excluding the channel generation. To be more precise, we present a comparison between the simulation time that is required by the EFDOM and that required by the exact model. Two different types of simulation time have been investigated—the channel-plus-ICI generation time, which is the time that is required to generate one realization of the useful channel vector and of the ICI vector, and the BER simulation time, which is the time that is required to simulate one coded BER iteration for a given SNR. We performed these simulations using the MathWorks software MATLAB version 7.0.4 on a PC with an Intel Xeon processor characterized by a 3-GHz clock frequency and a 2-GB RAM.

Fig. 8 displays the channel-plus-ICI generation time ratio (CTR) between the exact model and the EFDOM for the RA and BU channels as a function of the size N of the FFT. It is evident that the EFDOM efficiency gain is much greater for the BU channel, which has more paths than the RA. Specifically, the CTR for the BU is about 130, whereas it is approximately 15 for the RA. From Fig. 8, it is also clear that the CTR is practically independent from the FFT size. Fig. 8 also illustrates the BER simulation time ratio (BTR) between the exact model and the EFDOM for the RA and BU channels as a function of the FFT size N. In this case too, the EFDOM efficiency gain is much greater for the BU channel, with BTR $= 15$ for BU and BTR $= 3$ for RA, independently from the FFT size. Obviously, the BTR is lower than the CTR because the BTR also includes the channel decoding simulation time, which is the same for the two models and, consequently, has a bigger impact in the EFDOM BER simulation time than in the exact model. Fig. 9 shows the CTR as a function of the number L of channel paths. As expected, the simulation efficiency linearly increases with L.

VI. Conclusion

In this paper, we have proposed a novel simulation model, i.e., the EFDOM, to characterize the BER performance of COFDM systems in time-varying scenarios. The EFDOM allows for a faster BER simulation in Rayleigh and Rice channels, with a simulation efficiency that increases with the number of channel paths. Another merit of the EFDOM is the identification of few significant parameters that affect the coded BER performance. The proposed model can be useful for a detailed performance comparison among OFDM-based standards (like DAB, DVB-T/H, and T-DMB), which are expected to also work in mobile environments. The EFDOM could be useful also to develop an analytical BER performance analysis for those OFDM systems that employ coding strategies whose performance in Gaussian channels can be theoretically characterized with good accuracy.

Appendix A

In this Appendix, we derive the covariance matrix $\mathbf{C}_{\underline{\mathbf{h}}_U\underline{\mathbf{h}}_U} = E[\underline{\mathbf{h}}_U\underline{\mathbf{h}}_U^H]$ of the useful channel $\underline{\mathbf{h}}_U$. Since $\underline{\mathbf{h}}_U = [\mathbf{h}_U^T(1), \ldots, \mathbf{h}_U^T(N_S)]^T$, we can write

$$\mathbf{C}_{\underline{\mathbf{h}}_U\underline{\mathbf{h}}_U} = \begin{bmatrix} E\left[\mathbf{h}_U(1)\mathbf{h}_U^H(1)\right] & \cdots & E\left[\mathbf{h}_U(1)\mathbf{h}_U^H(N_S)\right] \\ \vdots & \ddots & \vdots \\ E\left[\mathbf{h}_U(N_S)\mathbf{h}_U^H(1)\right] & \cdots & E\left[\mathbf{h}_U(N_S)\mathbf{h}_U^H(N_S)\right] \end{bmatrix} \tag{28}$$

where, by exploiting the relation $\mathbf{h}_U(n) = \sqrt{N}\mathbf{F}\overline{\mathbf{h}}_T(n)$, each block can be expressed by

$$E\left[\mathbf{h}_U(n)\mathbf{h}_U^H(n+k)\right] = N\mathbf{F}E\left[\overline{\mathbf{h}}_T(n)\overline{\mathbf{h}}_T^H(n+k)\right]\mathbf{F}^H. \tag{29}$$

Since $\overline{\mathbf{h}}_T(n) = N^{-1}\sum_{i=L_{\mathrm{CP}}+1}^{N_T}\mathbf{h}_T(i+nN_T)$, the following holds true:

$$E\left[\overline{\mathbf{h}}_T(n)\overline{\mathbf{h}}_T^H(n+k)\right] = \sum_{i=L_{\mathrm{CP}}+1}^{N_T}\sum_{j=L_{\mathrm{CP}}+1}^{N_T}\frac{1}{N^2} \times E\left[\mathbf{h}_T(i+nN_T)\mathbf{h}_T^H(j+(n+k)N_T)\right] \tag{30}$$

where

$$E\left[\mathbf{h}_T(i+nN_T)\mathbf{h}_T^H\,(j+(n+k)N_T)\right] = J_0\left(2\pi\frac{\overline{f}_D}{N}(kN_T+j-i)\right)\mathbf{\Sigma} \quad (31)$$

and $\mathbf{\Sigma}$ denotes the power-delay profile matrix, which is diagonal because the channel taps are uncorrelated in the delay domain. By inserting (30) and (31) into (29), we obtain

$$E\left[\mathbf{h}_U(n)\mathbf{h}_U^H(n+k)\right] = \left[\overline{\mathbf{C}}_{\rm norm}\right]_{n,n+k}\mathbf{C}_{\mathbf{h}_U(n)\mathbf{h}_U(n)} \quad (32)$$

where $\overline{\mathbf{C}}_{\rm norm}$ is defined in (14), and $\mathbf{C}_{\mathbf{h}_U(n)\mathbf{h}_U(n)} = N\mathbf{F}\mathbf{\Sigma}\mathbf{F}^H$. By combining (32) with (28), we obtain the result of (13).

APPENDIX B

In this Appendix, we derive the ICI covariance matrix $\mathbf{C}_{\underline{\mathbf{i}}\underline{\mathbf{i}}}$. Since $\underline{\mathbf{i}} = \underline{\mathbf{P}}^T\underline{\mathbf{G}}^T\mathbf{n}_{\rm ICI}$, we have $\mathbf{C}_{\underline{\mathbf{i}}\underline{\mathbf{i}}} = \underline{\mathbf{P}}^T\underline{\mathbf{G}}^T\mathbf{C}_{\underline{\mathbf{n}}_{\rm ICI}\underline{\mathbf{n}}_{\rm ICI}}\underline{\mathbf{G}}\,\underline{\mathbf{P}}$, where

$$\mathbf{C}_{\underline{\mathbf{n}}_{\rm ICI}\underline{\mathbf{n}}_{\rm ICI}} = \begin{bmatrix} E\left[\mathbf{n}_{\rm ICI}(1)\mathbf{n}_{\rm ICI}^H(1)\right] & \cdots & E\left[\mathbf{n}_{\rm ICI}(1)\mathbf{n}_{\rm ICI}^H(N_S)\right] \\ \vdots & \ddots & \vdots \\ E\left[\mathbf{n}_{\rm ICI}(N_S)\mathbf{n}_{\rm ICI}^H(1)\right] & \cdots & E\left[\mathbf{n}_{\rm ICI}(N_S)\mathbf{n}_{\rm ICI}^H(N_S)\right] \end{bmatrix}. \quad (33)$$

We now observe that $E[\mathbf{n}_{\rm ICI}(n)\mathbf{n}_{\rm ICI}^H(k)] \cong \mathbf{0}_{N\times N}$ for $k \neq n$. Indeed

$$E\left[\mathbf{n}_{\rm ICI}(n)\mathbf{n}_{\rm ICI}^H(k)\right] = E\left[\mathbf{H}_I(n)\mathbf{x}(n)\mathbf{x}^H(k)\mathbf{H}_I^H(k)\right] = E\left[\mathbf{H}_I(n)\mathbf{C}_{\mathbf{x}(n)\mathbf{x}^H(k)}\mathbf{H}_I^H(k)\right] \quad (34)$$

where the data covariance $\mathbf{C}_{\mathbf{x}(n)\mathbf{x}^H(k)}$ imposed by the convolutional code is very weak and can be approximated as $\mathbf{C}_{\mathbf{x}(n)\mathbf{x}^H(k)} \cong \mathbf{0}_{N\times N}$ when $k \neq n$. Since $\mathbf{C}_{\mathbf{n}_{\rm ICI}(n)\mathbf{n}_{\rm ICI}^H(n)} = E[\mathbf{n}_{\rm ICI}(n)\mathbf{n}_{\rm ICI}^H(n)]$ is independent from the OFDM block index n, we can write

$$\mathbf{C}_{\underline{\mathbf{n}}_{\rm ICI}\underline{\mathbf{n}}_{\rm ICI}} = \mathbf{I}_{N_S}\otimes\mathbf{C}_{\mathbf{n}_{\rm ICI}(n)\mathbf{n}_{\rm ICI}^H(n)} \quad (35)$$

where $\mathbf{C}_{\mathbf{n}_{\rm ICI}(n)\mathbf{n}_{\rm ICI}^H(n)}$ is expressed by (34) with $k=n$. After the convolutional code, $\mathbf{C}_{\mathbf{x}(n)\mathbf{x}^H(n)} \cong \mathbf{I}_{N\times N}$, and hence, we approximate

$$\mathbf{C}_{\mathbf{n}_{\rm ICI}(n)\mathbf{n}_{\rm ICI}^H(n)} = \mathbf{F}E\left[\tilde{\mathbf{H}}_I(n)\tilde{\mathbf{H}}_I^H(n)\right]\mathbf{F}^H \quad (36)$$

where we exploited the relation $\mathbf{H}_I(n) = \mathbf{F}\tilde{\mathbf{H}}_I(n)\mathbf{F}^H$. To calculate the matrix $E[\tilde{\mathbf{H}}_I(n)\tilde{\mathbf{H}}_I^H(n)]$ in (36), we drop the OFDM block index n for notation simplicity, and we express $\tilde{\mathbf{H}}_I$ as follows:

$$\tilde{\mathbf{H}}_I = \tilde{\mathbf{H}} - \tilde{\mathbf{H}}_U = \sum_{l=0}^{L-1}\mathbf{D}_l\mathbf{Z}^l \quad (37)$$

where the circular-shift matrix $\mathbf{Z}$ is defined by $[\mathbf{Z}]_{j,k}=1$ for $j=(k+1) \bmod N$, and $[\mathbf{Z}]_{j,k}=0$ otherwise; $\mathbf{D}_l=\mathrm{Diag}(\mathbf{h}_l-\overline{h}_l\mathbf{1}_N)$ is a diagonal matrix; $\mathbf{h}_l=[h_l((n-1)N_T+L_{\rm CP}+1),\ldots,h_l(nN_T)]^T$; and $\overline{h}_l = N^{-1}\sum_{i=1}^{N}h_l((n-1)N_T+L_{\rm CP}+i)$. Clearly, $\mathbf{d}_l=\mathrm{diag}(\mathbf{D}_l)=\mathbf{h}_l-\overline{h}_l\mathbf{1}_N$ is the deviation from its average of the time-domain realization of the lth tap in the nth OFDM block. Since $[\mathbf{D}_l\mathbf{Z}^{l-j}\mathbf{D}_j^*]_{k,m} = [\mathbf{D}_l]_{k,k}[\mathbf{D}_j^*]_{m,m}$, for $k=(m+l-j) \bmod N$, and $[\mathbf{D}_l\mathbf{Z}^{l-j}\mathbf{D}_j^*]_{k,m}=0$ otherwise, by the independence of the channel taps in the delay domain, we obtain

$$E\left[[\mathbf{D}_l]_{k,k}\left[\mathbf{D}_j^*\right]_{k,k}\right] = 0 \quad (38)$$

when l is different from j. Hence, $E[\mathbf{D}_l\mathbf{Z}^{l-j}\mathbf{D}_j^*] = \mathbf{0}_{N\times N}$, and, therefore, $E[\tilde{\mathbf{H}}_I\tilde{\mathbf{H}}_I^H] = \sum_{l=0}^{L-1}E[\mathbf{D}_l\mathbf{D}_l^H]$. Consequently, the entries of the diagonal matrix $\mathbf{C}_{\tilde{\mathbf{H}}_I\tilde{\mathbf{H}}_I^H} = E[\tilde{\mathbf{H}}_I\tilde{\mathbf{H}}_I^H]$ can be expressed as follows:

$$\begin{aligned}\left[\mathbf{C}_{\tilde{\mathbf{H}}_I\tilde{\mathbf{H}}_I^H}\right]_{k,k} &= \sum_{l=0}^{L-1}\left\{E\left[h_l(k)h_l^*(k)\right] + \frac{1}{N^2}\sum_{m_1=1}^{N}\sum_{m_2=1}^{N}E\left[h_l(m_1)h_l^*(m_2)\right]\right\} \\ &= 1-\frac{2}{N}\sum_{m=1}^{N}J_0\left(2\pi f_D T_S(k-m)\right) + \frac{1}{N^2}\sum_{m_1=1}^{N}\sum_{m_2=1}^{N}J_0\left(2\pi f_D T_S(m_1-m_2)\right)\end{aligned} \quad (39)$$

since $\sum_{l=0}^{L-1}\sigma_l^2 = 1$. Interestingly, $N^{-1}\mathrm{tr}(\mathbf{C}_{\tilde{\mathbf{H}}_I\tilde{\mathbf{H}}_I^H}) = P_{\rm ICI}$, where $P_{\rm ICI}$ is expressed by (7). Summarizing

$$\mathbf{C}_{\underline{\mathbf{i}}\underline{\mathbf{i}}} = \underline{\mathbf{P}}^T\underline{\mathbf{G}}^T\left(\mathbf{I}_{N_S}\otimes\mathbf{F}\mathbf{C}_{\tilde{\mathbf{H}}_I\tilde{\mathbf{H}}_I^H}\mathbf{F}^H\right)\underline{\mathbf{G}}\,\underline{\mathbf{P}} \quad (40)$$

where $\mathbf{C}_{\tilde{\mathbf{H}}_I\tilde{\mathbf{H}}_I^H}$, expressed by (39), depends on the Doppler spread and is independent of the power-delay profile.

APPENDIX C

When $N_S=1$, the pdf of $\varphi^{(E)}$ can be analytically derived. In this case, (20) becomes

$$\varphi^{(E)} = \sum_{l=0}^{L-1}\left|h_l^{(E)}-m_l\right|^2 \quad (41)$$

where $h_l^{(E)}$ is a random variable with the same statistical properties of the lth channel path. For Rayleigh channels, the terms $\{|h_l^{(E)}|^2\}$ are exponentially distributed, with parameters $\{\lambda_l = 1/\sigma_l^2\}$, $l=0,\ldots,L-1$. Since the channel taps are uncorrelated in the delay domain, the random variables $\{|h_l^{(E)}|^2\}$ are mutually *independent*. From [23], it is possible to show that

TABLE I
VALUES OF ρ_P FOR $N_S = 4$

$f_D/\Delta f$	RA (Simulated)	BU (Simulated)	Theoretical
1.25 %	-0.0149	0.0315	0.0082
2.5 %	0.0038	0.0287	0.0330
3.5 %	0.0567	0.0269	0.0647
5 %	0.1025	0.0682	0.1318
7 %	0.2502	0.2482	0.2540
10 %	0.4565	0.4679	0.4713
14 %	0.6472	0.6547	0.6649
20 %	0.6598	0.6778	0.6904
28 %	0.7154	0.6965	0.7260
40 %	0.6445	0.6387	0.6698
45 %	0.4691	0.4125	0.4952
50 %	0.2214	0.1863	0.2761
56 %	0.0822	0.0964	0.1701

the pdf of the sum of independent exponential random variables is expressed by

$$f_{\varphi^{(E)}}\left(\varphi^{(E)}\right) = \left[\prod_{l=0}^{L-1}\lambda_l\right]\cdot\sum_{j=0}^{L-1}\frac{e^{-\lambda_j\varphi^{(E)}}}{\prod\limits_{\substack{k=0\\k\neq j}}^{L-1}(\lambda_k-\lambda_j)},\quad \varphi^{(E)}\geq 0 \tag{42}$$

which is very close to $f_\varphi(\varphi)$ (we have verified this by extensive simulations, summarized by Fig. 2). It is worth noting that, for $N_S > 1$, the exponential random variables are correlated, and hence, (42) is not valid.

APPENDIX D

In this Appendix, we give some details about the superblock correlation coefficient ρ_P expressed by (22). The complete derivation of ρ_P can be found in [24] for the specific case $N_S = 4$. Anyway, the same procedure of [24] can be used for any value of N_S. The final result of this procedure is given by

$$\rho_P = \frac{N_S\left\|\mathbf{c}(0)\right\|^2 + 2\sum\limits_{n=1}^{N_S-1}\left((N_S-n)\left\|\mathbf{c}(n)\right\|^2\right)}{\sqrt{\left(N_S\left\|a(0)\right\|^2 + 2\sum\limits_{n=1}^{N_S-1}\left((N_S-n)\left\|a(n)\right\|^2\right)\right)}} \times \frac{1}{\sqrt{\left(N_S\left\|\mathbf{B}(0)\right\|^2 + 2\sum\limits_{n=1}^{N_S-1}\left((N_S-n)\left\|\mathbf{B}(n)\right\|^2\right)\right)}} \tag{43}$$

where

$$\mathbf{c}(n) = \mathbf{a}(n) - a(n)\mathbf{1}_N \tag{44}$$

$$[\mathbf{a}(n)]_{i+1} = \frac{1}{N}\sum_{k=0}^{N-1}J_0\left(2\pi\frac{\overline{f}_D}{N}|i-k+nN_T|\right)\qquad i=0,\ldots,N-1 \tag{45}$$

$$a(n) = \frac{1}{N}\mathbf{1}_N^T\mathbf{a}(n) \tag{46}$$

$$[\mathbf{B}(n)]_{i+1,j+1} = J_0\left(2\pi\overline{f}_D|i-j|/N\right) + a(n) - [\mathbf{a}(n)]_j - [\mathbf{a}(n)]_{N-i}\qquad i,j=0,\ldots,N-1. \tag{47}$$

When $N_S = 1$, numerical calculation shows that $0 \leq \rho_P \leq 0.0542$ for a wide range of normalized Doppler spreads, which are expressed by $0 \leq \overline{f}_D \leq 0.56$. Hence, when $N_S = 1$, the superblock correlation coefficient $\rho_P \cong 0$ can be safely omitted. When $N_S > 1$, the correlation coefficient ρ_P can be significantly different from zero. Anyway, the analytical value of ρ_P is very close to the simulated values. This is shown in Table I for $N_S = 4$ for both BU and RA channels, thus confirming the independence of ρ_P from the power-delay profile.

REFERENCES

[1] L. J. Cimini, "Analysis and simulation of a digital mobile channel using orthogonal frequency division multiplexing," *IEEE Trans. Commun.*, vol. COM-33, no. 7, pp. 665–675, Jul. 1985.

[2] *Digital Video Broadcasting (DVB); Framing Structure, Channel Coding and Modulation for Digital Terrestrial Television*, ETSI EN 300 744 V1.5.1, Nov. 2004.

[3] *Digital Audio Broadcasting (DAB); Data Broadcasting—MPEG-2 TS Streaming*, ETSI TS 102 427 V1.1.1, Jul. 2004.

[4] *Part 11: Wireless LAN Medium Access Control (MAC) and Physical Layer (PHY) Specifications: High-speed Physical Layer in the 5 GHz Band*, IEEE Std. 802.11a-1999, Sep.1999.

[5] *IEEE standard for Local and Metropolitan Area Networks, Part 16: Air Interface for Fixed and Mobile Broadband Wireless Access Systems*, IEEE Std. 802.16e-2005, Feb. 2006.

[6] M. Russell and G. L. Stüber, "Interchannel interference analysis of OFDM in a mobile environment," in *Proc. IEEE Veh. Technol. Conf.*, Jul. 1995, vol. 2, pp. 820–824.

[7] P. Robertson and S. Kaiser, "The effects of Doppler spreads in OFDM(A) mobile radio systems," in *Proc. IEEE Veh. Technol. Conf.—Fall*, Sep. 1999, vol. 1, pp. 329–333.

[8] E. Chiavaccini and G. M. Vitetta, "Error performance of OFDM signaling over doubly-selective Rayleigh fading channels," *IEEE Commun. Lett.*, vol. 4, no. 11, pp. 328–330, Nov. 2000.

[9] Y. Li and L. J. Cimini, "Bounds on the interchannel interference of OFDM in time-varying impairments," *IEEE Trans. Commun.*, vol. 49, no. 3, pp. 401–404, Mar. 2001.

[10] T. Wang, J. G. Proakis, E. Masry, and J. R. Zeidler, "Performance degradation of OFDM systems due to Doppler spreading," *IEEE Trans. Wireless Commun.*, vol. 5, no. 6, pp. 1422–1432, Jun. 2006.

[11] M. Poggioni, L. Rugini, and P. Banelli, "A novel simulation model for coded OFDM in Doppler scenarios: DVB-T versus DAB," in *Proc. IEEE Int. Conf. Commun.*, Glasgow, U.K., Jun. 2007, pp. 5689–5694.

[12] COST 207, *Digital Land Mobile Radio Communications*, 1989, Luxembourg: Office Official Pubs. Eur. Communities. Final Rep.

[13] P. Bello, "Characterization of randomly time-variant linear channels," *IEEE Trans. Commun.*, vol. COM-11, no. 4, pp. 360–393, Dec. 1963.

[14] Y. R. Zheng and C. Xiao, "Improved models for the generation of multiple uncorrelated Rayleigh fading waveforms," *IEEE Commun. Lett.*, vol. 6, no. 6, pp. 256–258, Jun. 2002.

[15] Z. Wang and G. B. Giannakis, "Wireless multicarrier communications," *IEEE Signal Process. Mag.*, vol. 17, no. 3, pp. 29–48, May 2000.

[16] G. H. Golub and C. F. Van Loan, *Matrix Computations*, 3rd ed. Baltimore, MD: Johns Hopkins Univ. Press, 1996.

[17] J. G. Proakis, *Digital Communications*, 4th ed. New York: McGraw-Hill, 2001.

[18] W. C. Lee, H. M. Park, and J. S. Park, "Viterbi decoding method using channel state information in COFDM system," *IEEE Trans. Consum. Electron.*, vol. 45, no. 3, pp. 533–537, Aug. 1999.

[19] A. V. Oppenheim and R. W. Schafer, *Discrete-Time Signal Processing*. Englewood Cliffs, NJ: Prentice-Hall, 1989.

[20] J. Jootar, J. R. Zeidler, and J. G. Proakis, "Performance of finite-depth interleaved convolutional codes in a Rayleigh fading channel with noisy channel estimates," in *Proc. IEEE Veh. Technol. Conf.—Spring*, May–Jun. 2005, vol. 1, pp. 600–605.

[21] J. K. Cavers and P. Ho, "Analysis of the error performance of trellis-coded modulations in Rayleigh-fading channels," *IEEE Trans. Commun.*, vol. 40, no. 1, pp. 74–83, Jan. 1992.
[22] Z. Wang and G. B. Giannakis, "A simple and general parameterization quantifying performance in fading channels," *IEEE Trans. Commun.*, vol. 51, no. 8, pp. 1389–1398, Aug. 2003.
[23] S. V. Amari and R. B. Misra, "Closed-form expressions for distribution of sum of exponential random variables," *IEEE Trans. Rel.*, vol. 46, no. 4, pp. 519–522, Dec. 1997.
[24] M. Poggioni, L. Rugini and P. Banelli, "A novel simulation model for coded OFDM in Doppler scenarios: DVB-T/H versus T-DMB," Dept. Elect. Inform. Eng, Perugia, Italy, Tech. Rep. RT-004-06. Oct. 2006. [Online]. Available: http://www.diei.unipg.it/rt/RT-004-06-Poggioni-Rugini-Banelli.pdf

Mario Poggioni (S'07) was born in Perugia, Italy, in 1979. He received the Laurea degree (*cum laude*) in electronics engineering from the University of Perugia in 2005, where he is currently working toward the Ph.D. degree with the Department of Electronic and Information Engineering.

His research interests include the areas of signal processing for multicarrier communications, fast-fading channels, broadcasting, and cross-layer designs.

Luca Rugini (S'01–M'05) was born in Perugia, Italy, in 1975. He received the Laurea degree in electronics engineering and the Ph.D. degree in telecommunications from the University of Perugia in 2000 and 2003, respectively.

From February to July 2007, he visited Delft University of Technology, Delft, The Netherlands. He is currently a Postdoctoral Researcher with the Department of Electronic and Information Engineering, University of Perugia. His research interests include the area of signal processing for multicarrier and spread-spectrum communications.

Paolo Banelli (S'90–M'99) received the Laurea degree in electronics engineering and the Ph.D. degree in telecommunications from the University of Perugia, Perugia, Italy, in 1993 and 1998, respectively.

In 1998, he was an Assistant Professor with the Department of Electronic and Information Engineering, University of Perugia, where he has been an Associate Professor since 2005. In 2001, he joined the SpinComm group at the Department of Electrical and Computer Engineering, University of Minnesota, Minneapolis, as a Visiting Researcher. His research interests include nonlinear distortions, broadcasting, time-varying channel estimation and equalization, and block-transmission techniques for wireless communications. He has been serving as a Reviewer for several technical journals and as a Technical Program Committee Member of leading international conferences on signal processing and telecommunications.